Crystal structure of a new heat-labile enterotoxin, LT-IIb

Focco van den Akker[1], Steve Sarfaty[1,2], Edda M Twiddy[3], Terry D Connell[3†], Randall K Holmes[3‡] and Wim GJ Hol[1,2*]

Background: Cholera toxin from *Vibrio cholerae* and the type I heat-labile enterotoxins (LT-Is) from *Escherichia coli* are oligomeric proteins with AB_5 structures. The type II heat-labile enterotoxins (LT-IIs) from *E. coli* are structurally similar to, but antigenically distinct from, the type I enterotoxins. The A subunits of type I and type II enterotoxins are homologous and activate adenylate cyclase by ADP-ribosylation of a G protein subunit, $G_s\alpha$. However, the B subunits of type I and type II enterotoxins differ dramatically in amino acid sequence and ganglioside-binding specificity. The structure of LT-IIb was determined both as a prototype for other LT-IIs and to provide additional insights into structure/function relationships among members of the heat-labile enterotoxin family and the superfamily of ADP-ribosylating protein toxins.

Results: The 2.25 Å crystal structure of the LT-IIb holotoxin has been determined. The structure reveals striking similarities with LT-I in both the catalytic A subunit and the ganglioside-binding B subunits. The latter form a pentamer which has a central pore with a diameter of 10–18 Å. Despite their similarities, the relative orientation between the A polypeptide and the B pentamer differs by 24° in LT-I and LT-IIb. A common hydrophobic ring was observed at the A–B_5 interface which may be important in the cholera toxin family for assembly of the AB_5 heterohexamer. A cluster of arginine residues at the surface of the A subunit of LT-I and cholera toxin, possibly involved in assembly, is also present in LT-IIb. The ganglioside receptor binding sites are localized, as suggested by mutagenesis, and are in a position roughly similar to the sites where LT-I binds its receptor.

Conclusions: The structure of LT-IIb provides insight into the sequence diversity and structural similarity of the AB_5 toxin family. New knowledge has been gained regarding the assembly of AB_5 toxins and their active-site architecture.

Addresses: [1]Departments of Biological Structure and Biochemistry & Biomolecular Structure Center, University of Washington, [2]Howard Hughes Medical Institute, University of Washington, Box 357742, Seattle, WA 98195, USA and [3]Department of Microbiology and Immunology, Uniformed Services University of the Health Sciences, Bethesda, MD 20814, USA.

Present addresses: [†]Department of Microbiology, School of Medicine and Biomedical Sciences, Buffalo, NY 14214-3078, USA and [‡]Department of Microbiology, University of Colorado Health Sciences Center, Denver, CO 80262, USA.

*Corresponding author.
E-mail: hol@xray.bmsc.washington.edu

Key words: ADP-ribosylation, bacterial toxins, ganglioside receptor, X-ray structure

Received: 14 Feb 1996
Revisions requested: 12 Mar 1996
Revisions received: 28 Mar 1996
Accepted: 28 Mar 1996

Structure 15 June 1996, 4:665–678

Introduction

Escherichia coli heat-labile enterotoxins (LTs) are closely related to cholera toxin (CT) in both structure and modes of action [1,2]. Both toxins act on intestinal epithelial cells, causing a diarrheal disease in humans. They belong to the AB class of bacterial toxins and have an AB_5 structure. The A subunit of LT and CT catalyzes the ADP-ribosylation of a G protein subunit, $G_s\alpha$, and their B subunits form a pentamer responsible for the recognition of the specific ganglioside receptors. After binding to the ganglioside receptor on the epithelial cells, the A subunit is endocytosed. Inside the cell the A1 subunit ADP-ribosylates the α subunit of the heterotrimeric G-protein G_s. In order to become fully active, the A subunit needs to be proteolytically cleaved and reduced, resulting in an active A1 subunit and a smaller 45-residue A2 'linker' which is responsible for associating the A subunit and the B pentamer.

The crystal structures of both the type I heat-labile enterotoxin (LT-I) and the very similar CT have been determined, revealing a doughnut-shaped B pentamer, a wedge-shaped A1 subunit and an A2 linker holding on to the B pentamer by penetrating its pore [3–8]. Unlike LT-I and CT, type II heat-labile enterotoxins (LT-IIa and LT-IIb) were isolated and characterized more recently [9–11]. LT-II-producing *E. coli* can be isolated from cows, buffalo, and pigs, but rarely from humans [12–14]. Interestingly, LT-IIs are 25–50-fold more toxic to Y1 mouse adrenal tumor cells than LT-I, although they are not active in the *in vivo* rabbit ligated ileal segment assay [15,16]. LT-IIs have been shown to bind to intestinal cells [17], but their role in pathogenesis of infectious diseases caused by *E. coli* remains to be established.

LT-IIs share many features with LT-I and CT. These include the AB_5 architecture and the ability to activate adenylate cyclase by ADP-ribosylating the same target, the G-protein subunit $G_s\alpha$ [18,19]. The amino acid sequence of the catalytic A1 subunits of LT-IIa and LT-IIb are 85% identical, and share about 63% sequence identity with LT-I.

However, the A2 linkers share only 38% sequence identity between LT-IIa and LT-IIb and have only 21% sequence identity with LT-I [10,11]. The B subunits of LT-IIa and LT-IIb show 58% sequence identity to each other; however, they show no detectable sequence similarity to the LT-I B subunit. This is also reflected in the fact that LT-IIa and LT-IIb have been shown to have different ganglioside specificities from LT-I. LT-IIb binds to gangliosides G_{D1a} and G_{T1b} and weakly to G_{M3}. LT-IIa binds a larger variety of gangliosides, with the highest affinity for G_{D1b}, followed by G_{D1a}, G_{T1b}, G_{Q1b}, G_{M1}, G_{D2}, G_{M2}, and G_{M3} [20]. Interestingly, all the listed gangliosides which bind to LT-IIa and LT-IIb are able to suppress an immune response in humans by inhibiting T-cell responses. Tumor cells shed these gangliosides from their surfaces creating a highly immunosuppressive microenvironment [21]. Several of these gangliosides (G_{D2}, G_{M2} and G_{M3}) have been used as targets for cancer therapy using monoclonal antibodies and/or for active specific immunotherapy with vaccines [22,23]. Heat-labile enterotoxins are not the only molecules to make use of gangliosides for recognition of their target cells: botulinum A neurotoxin recognizes G_{T1b} and G_{D1a} [24] and the Sendai virus can use G_{D1a} as a receptor [25].

We have determined the crystal structure of LT-IIb at 2.25 Å resolution. Although its role in pathogenesis of infectious diarrheal diseases in humans or animals remains to be established, the LT-IIb structure can aid elucidation of common features in the interactions between the A subunit and the B pentamer in the cholera toxin family. This LT-IIb structure further increases our understanding of the still unknown catalytic mechanism of ADP-ribosylating toxins. The structure may also provide new insights into the special characteristics of type II enterotoxins, such as their increased toxicity for mouse Y1 adrenal tumor cells [15] and their ability to bind to several cancer-associated gangliosides [22,23].

Results and discussion

Structure determination

The structure of LT-IIb was determined in a non-standard way using a combination of a single isomorphous K_2PtCl_4 derivative (Table 1), a homology model of the A1 and A2 subunits, and exploitation of the fivefold non-crystallographic symmetry present in the B pentamer. An initial 5 Å single isomorphous replacement (SIR) electron-density map revealed the presence of five rods along a fivefold axis (Fig. 1a). These rods could be superimposed onto the five long α helices of the B pentamer of LT-I, giving a first indication of structural similarity between LT-IIb and LT-I. A sixth long rod representing the long A2 helix was also clearly visible in the same SIR map (Fig. 1a). Solvent flattening, histogram matching, phase extension, and fivefold averaging improved the electron density within the B pentamer sufficiently for model building. For the A subunit, an initial homology model was built using the LT-I structure as a starting point. This A-subunit model could be placed in the asymmetric unit because the roughly triangular shape of the A subunit and the location of the A2 helix could be used to guide manual positioning in the 5 Å electron-density map. Rigid-body refinement in X-PLOR [26] followed by conventional refinement and several rounds of model building resulted in an R-factor of 19.1% for data from 10.0–2.25 Å resolution (Table 2).

Table 1

X-ray data collection statistics.

	Native 1	K_2PtCl_4	Native 2
Diffraction limit (Å)	2.5	3.3	2.25
Completeness (%) (final shell)	85 (65)	67 (44)	83 (68)
R_{merge}* (%)	7.9	11.8	6.3
R_{iso}† (%) (15–4 Å)	–	14.8	
Phasing power‡ (10–5 Å)			
acentric	–	1.7	
centric	–	1.4	
R_{cullis}§ (%) (10–5 Å)			
acentric	–	0.71	
centric	–	0.56	
Number of sites	–	7	

*$R_{merge}=\Sigma|I-<I>|/\Sigma I$. †$R_{iso}=\Sigma|F_{PH}-F_P|/\Sigma F_P$. ‡Phasing power=root mean square (rms) f_H/E, where f_H=calculated heavy-atom structure-factor amplitude and E=lack of closure=$\Sigma||F_{PH}\pm F_P|-f_H|$, where F_{PH}=structure-factor amplitude of the derivative crystal and F_P=structure-factor amplitude of the native crystal. §R_{cullis}=lack of closure/isomorphous difference.

Figure 1b shows a typical portion of the final $2F_o-F_c$ map calculated using data from 20–2.25 Å resolution. The final model includes residues 1–98 of each B subunit, residues 1–46 and 48–187 of the A1 subunit and residues 195–230 of the A2 linker. The C-terminal Glu99 in each of the five B subunits is disordered and thus not included. Residues 188–194, comprising the putative cleavage site in the A-subunit analogues to LT-I, could not be located in the electron-density map. Residue Ala47 in the A subunit was too disordered to be modeled properly and is thus not included in the model. In addition, the C-terminal residues 231–243 of the A2 chain could not be traced. However, substantial yet uninterpretable electron density in the pore persists in F_o-F_c maps contoured at the 2σ level, indicating a partially disordered conformation for these terminal residues.

Overall structure

The structure of LT-IIb is very similar to LT-I (Figs 2,3). The catalytic A subunit adopts the same fold in the two toxins with a characteristic wedge-shaped structure. The A subunit sits on top of the ring-like B pentamer. The B subunits follow the fivefold symmetry almost perfectly and are virtually identical to each other, as will be described in more detail below. Along the side of the A1 subunit 'rests' the A2 subunit as one long helix. This A2 helix penetrates the pore of the B pentamer and continues

Figure 1

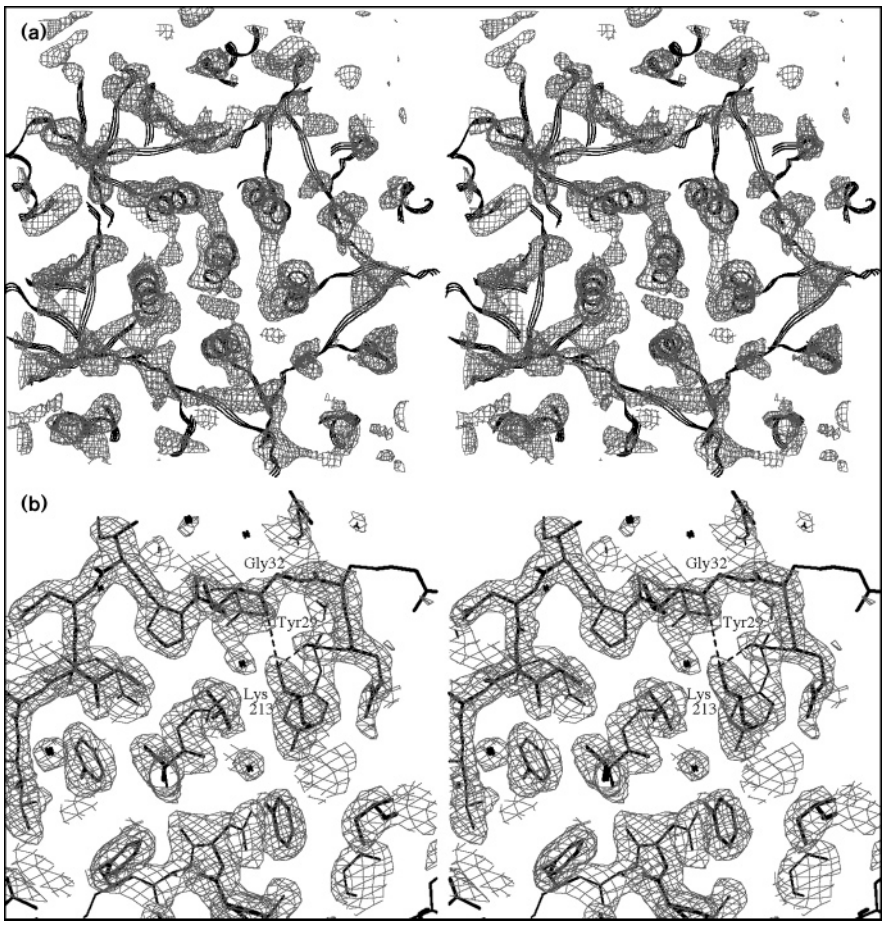

Electron-density maps of LT-IIb. (a) A stereo diagram showing a 5 Å SIR electron-density map. This map is contoured at 1.5σ and reveals five long rods representing the helices around the pore of the pentamer of LT-IIb. Part of the A2 helix in the middle of the pore is also visible. The superimposed ribbon tracings are of the final LT-IIb structure. (b) Final $2F_o–F_c$ map contoured at 1.5σ, depicting part of the A subunit, in particular residues 29–37. The interaction of Lys213 of the A2 subunit with the carbonyl oxygens of Tyr29 and Gly32 are indicated by dashed lines. The Nζ to oxygen hydrogen bonds are 2.8 and 3.1 Å, respectively.

to about halfway down the pore. The A2 linker provides almost all the interactions between the A subunit and the pentamer. The A1 subunit does not make many direct interactions with the B pentamer, except for Arg145, which participates in three hydrogen bonds. The LT-I A1 subunit makes more interactions by means of Arg33, Arg148 and Arg151, which are involved in salt bridges with the pentamer. Concerning the loop in the A1 subunit near residue 145, it has been shown in LT-I that four arginines located between residues 141 and 148 are important for AB_5 formation, although each individual arginine can be mutated without any noticeable effect [27]. In the LT-IIb sequence there are also four arginine residues (although one of them is not in the equivalent position), confirming their importance. Interestingly, the orientation of the A subunit with respect to the B pentamer is quite different in the two enterotoxins. A rotation of 24° has to be applied to the A subunit of LT-IIb for it to have the same relative orientation, with respect to its B pentamer, as in LT-I. A variable A/B_5 orientation is also observed in different crystal forms of LT-I [28]. Not only the orientation but also the mode of association between the A2 subunit and the B pentamer in LT-IIb are distinctly different from those for LT-I, and these will be discussed below in more detail.

Table 2

Summary of refinement statistics.

Resolution range (Å)	10–2.25
Unique reflections (F>2σF)	43 325
Protein atoms	5469
Solvent molecules	215
R-factor (%)	19.1
R_{free} (%) (10–2.5 Å)	26.6
Rms coordinate error (Å)*	0.28
Rms deviation from ideality	
bonds (Å)	0.011
angles (°)	1.8
dihedral angles (°)	23.7

*Obtained from a Luzzati plot.

Unlike diphtheria toxin (DT) and *Pseudomonas aeruginosa* exotoxin A (ETA), the membrane translocation of CT does not require entry into acidic vesicles [29], although earlier reports suggested such an acid-triggered mechanism

Figure 2

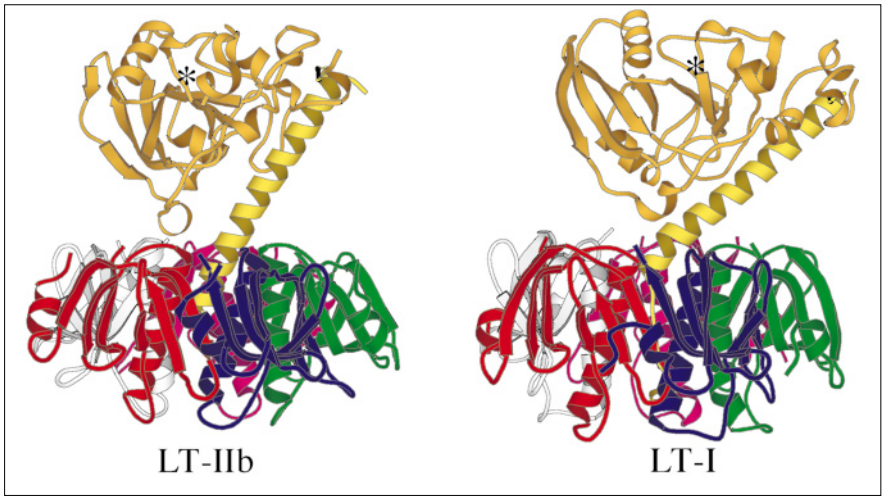

The structures of LT-IIb and LT-I. The A1 subunit is shown in gold and the A2 subunit in yellow. LT-IIb (left) and LT-I (right) holotoxins [3,4] are viewed such that their B pentamers are in a similar orientation. The individual B subunits are in red, white, pink, green and blue. The active-site region of each molecule is highlighted by an asterisk and the disulphide bond in the A subunit is indicated by a black line. (Figure generated using MOLSCRIPT [68].)

[30]. Our structure of LT-IIb was determined at pH 4.4, being the first low pH structure to be reported for a member of the CT family. The fact that our structure is very similar to those of CT and LT-I, determined at neutral pH, supports the observation that a low pH is not required for A-subunit translocation and processing.

Figure 3

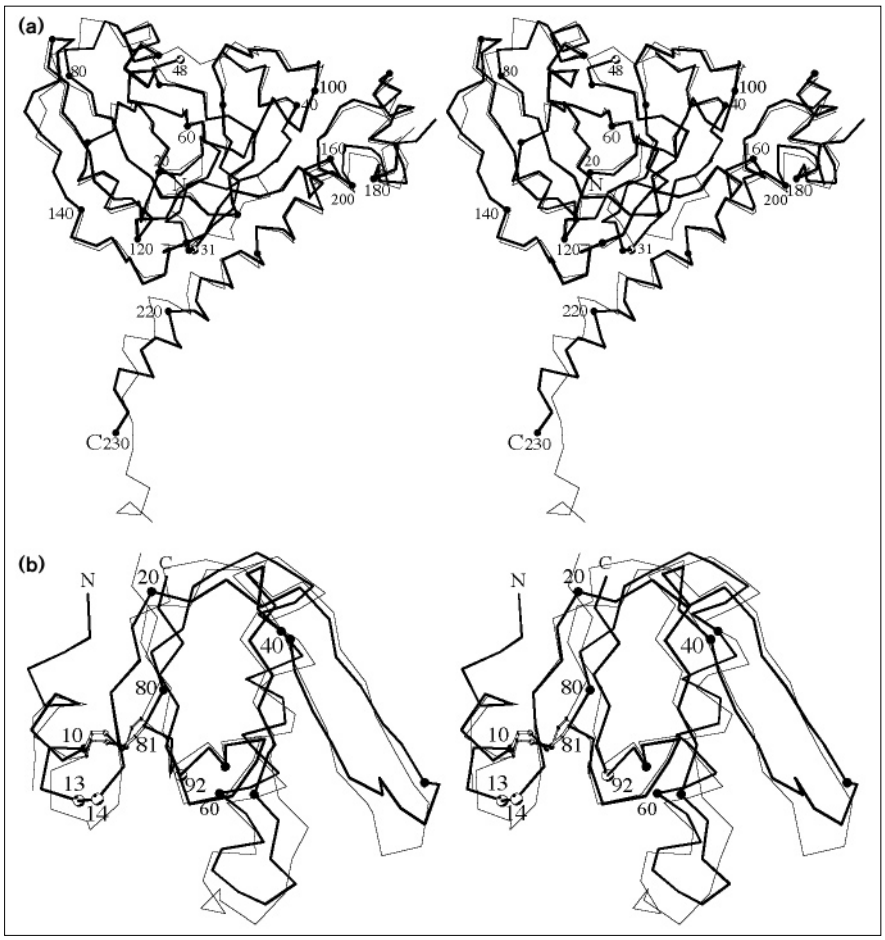

Structures of the A and B subunits of LT-IIb and LT-I. (a) Stereo diagram showing the superposition of the A subunits of LT-IIb and LT-I. LT-IIb is shown as thick lines while LT-I [3,4] is shown as thin lines. The N and C termini and the position of every twentieth residue in the LT-IIb structure are labeled. Also highlighted are residues 31 and 48 indicating the position of loops 24–34 and 45–54. The importance of these loops is discussed in the text. The C terminus indicated at position 230 is not the true C terminus, as the last 13 residues were not visible. (b) Stereo diagram showing the superposition of the B subunit of LT-IIb and LT-I [3,4]. The N and C termini and the position of every twentieth residue in LT-IIb are indicated. The disulphide bridges in both B subunits are also shown, the cysteine residues are shown in ball-and-stick representation. The positions of residues 13, 14 and 92 are highlighted by white spheres: their importance is discussed in the text.

The A subunit

The A subunit of LT-IIb is very similar to that of LT-I (Fig. 3a). Superimposing LT-IIb (residues 2–23, 35–46 and 48–186) onto their equivalent residues in LT-I results in a root mean square (rms) deviation of 0.77 Å for 173 Cα atoms, with a sequence identity of 64%. However, the conformation of loop 24–34 in LT-IIb is substantially different from the conformation observed in LT-I (Fig. 3a). The significantly different loop conformation is reflected in a much larger rms deviation of 4.49 Å for the Cα atoms of these 11 residues, with the largest difference being 6.2 Å. When comparing LT-IIb and LT-I loop 24–34 is 45% identical in amino acid sequence. The precise cause of the large difference in conformation of this loop is not obvious except for the fact that this stretch of residues has diverged more in amino acid sequence than the rest of the A1 subunit.

In the activation site of LT-IIb, the Cys185–Cys197 disulfide bridge is located at the same position as in LT-I. As in LT-I, the cleavage site in LT-IIb is flexible, since residues 188–194 could not be located in the electron-density map. The conserved mobility in the cleavage loop indicates that this flexibility is needed for proper proteolytic cleavage and activation in heat-labile enterotoxins. The overall temperature factor for the LT-IIb A1 subunit is 24 $Å^2$. This is lower than that observed in the LT-I structure (38 $Å^2$) [4]. There might be several reasons for this observation such as differences in the inherent mobility of the A subunit, as well as differences in crystal packing. However, the average temperature factors for main-chain atoms per residue show a similar, but not identical, trend, as seen in the LT-I structure.

The active site is located in a cleft on the A subunit remote from the B pentamer (Fig. 2). The active site in both CT and LT-I has been under investigation by means of mutagenesis. Besides the critically conserved Glu112 [31,32], substitutions of the following residues have been shown to affect ADP-ribosylation: Arg7, Asp9, His44, Ser61, Ser63, Val97, Tyr104, Pro106, His107, Glu110 and Ser114 [33–40]. The active site in LT-I is partially occluded by a 10-residue loop comprising residues 47–56. This loop in LT-I has been postulated to significantly alter its position upon activation of the toxin in order to accommodate NAD access to the active site [6]. In the LT-IIb holotoxin structure, this loop is in a virtually identical location, also rendering the active site partially inaccessible to the substrates (Figs 3a,4). Arg5 of LT-IIb, which is equivalent to Arg7 in LT-I, is involved in identical interactions with this loop via two hydrogen bonds formed with carbonyl atoms of Thr51 and Arg52. Arg7 in LT-I has been proposed to have a dual function: to hold loop 47–56 down in the AB_5 holotoxin, thus rendering the active site inaccessible, and to interact with NAD once LT-I is activated and loop 47–56 has been reorganized [6].

Figure 4

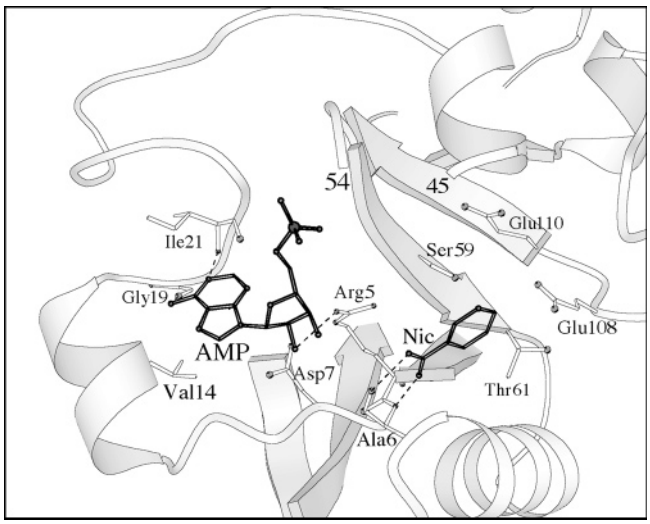

Schematic diagram showing the position of the AMP and nicotinamide (Nic) moieties of NAD, within the active site of LT-IIb, and their postulated interactions based upon similar interactions found with these moieties in exotoxin A [40]. For clarity, residues comprising loop 45–54 are omitted in this figure; labels (45 and 54) have been placed to indicate the beginning and the end of this loop. Some additional minor structural adjustments, such as displacement of Arg9 (not shown), are likely to occur to accommodate NAD binding. The catalytic glutamic acid, Glu110, is also highlighted.

The position and postulated interactions of the AMP and nicotinamide moieties of NAD with the A subunit of LT-IIb, as extrapolated from the ETA-complexed structure [41], are shown in Figure 4. Loop 45–54 is omitted from the figure for clarity. The following specific interactions are postulated to occur: First, the amide moiety of nicotinamide is hydrogen bonded to the backbone oxygen and nitrogen of Ala6; second, the ribose moiety of adenosine forms hydrogen bonds with Arg5 and Asp7; third, the adenine moiety interacts with the backbone oxygen of the fully conserved Gly19 and with the nitrogen of Ile21; fourth, Val14 provides a hydrophobic interaction with the adenine ring. The binding mode of NAD in the active site agrees well with the mutagenesis results carried out in each of the toxins.

The ETA structure, in complex with NAD fragments, [41] highlighted two important stretches of residues (residues 12–14 and 19–22) which had not previously been included in any of the published structure alignments performed on the whole family of ADP-ribosylating toxins. The catalytic residue Glu110 (which corresponds to Glu112 in LT-I and CT) was the first residue known to be conserved throughout this family. The structure-based sequence alignment, as shown in Figure 5, reveals the presence of a second fully conserved residue: the glycine at position 19 in the LT-IIb sequence. In both the complexed structure of DT

Figure 5

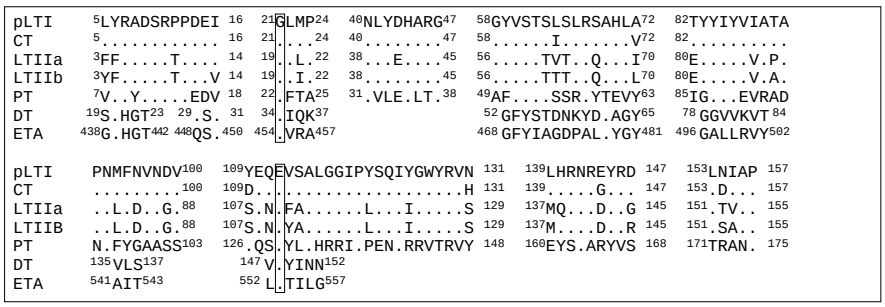

Structure based sequence alignment of the catalytic subunits of members of the ADP-ribosyltranferase toxin family. Sequences are aligned from porcine LT-I [4], CT [8], LT-IIa (though no structure of this toxin is available yet), LT-IIb, PT (pertussis toxin) [43], DT (diptheria toxin) [42] and ETA (exotoxin A) [41]. The two fully conserved residues are shown boxed. The residues that are not in structurally equivalent positions are not shown in this figure.

(with adenylyl 3′-5′ uridine 3′ monophosphate [ApUp] [42]) and ETA (with NAD fragments [41]) this conserved glycine adopts ϕ and ψ angles (138° and 151° in DT, 105° and 159° in ETA) which are energetically unfavorable for any other amino acid. The corresponding ϕ and ψ angles for Gly19 in LT-IIb, which does not have an adenosine fragment bound, are roughly similar (153° and –164° respectively) to those angles observed in DT and ETA, although not identical. The reason that a glycine is strictly conserved at this position is most likely because the ϕ and ψ angles, which for all other residues are unfavorable, need to be such that both the backbone oxygen and nitrogen atoms are correctly oriented to make two important interactions. The first of these interactions is a hydrogen bond between the backbone oxygen and the N6 atom of the adenine moiety of NAD (Fig. 4); the second is a hydrogen bond between its backbone nitrogen and the backbone oxygen of a valine residue (Val14 in LT-IIb). The second interaction is present in all structures of the above-mentioned ADP-ribosylating toxins (LT-I, CT, DT, ETA), pertussis toxin (PT) [43], and LT-IIb reported in this paper. As described above, Val14 is postulated, based upon the corresponding isoleucine residues in ETA and DT (see Fig. 4), to be involved in a hydrophobic interaction with the adenine ring of NAD. The sequence alignment in Figure 5 shows that the variation of the chemical nature of the residue at position 14 (of LT-IIb) is extremely limited since in the family of ADP-ribosyltransferase toxins, only a valine or an isoleucine is observed at this position. In conclusion, the NAD-binding mode in LT-IIb and LT-I, as extrapolated from the AMP/nicotinamide/ETA structure, is in good agreement both with mutagenesis data and the conservation of the critical residues Gly19 and Val/Ile (at position 14 of LT-IIb). Both these conserved residues are involved in interactions with the adenine moiety of NAD, throughout the toxin family ([44]; see note added in proof).

In LT-I a pathway of activation leading from the cleavage site to the active site has been proposed to be mediated via, sequentially, the A2 helix, loop 25–36 and loop 47–56 [6]. Two critical interactions in this putative cascade of conformational changes in LT-I are conserved in LT-IIb: the hydrogen bond between the main chain N of Arg23 with O of Tyr53; and the interaction between loop 24–34 and the A2 helix. However, the precise nature of these interactions is substantially different in LT-IIb compared with LT-I. Both the hydrophobic interactions (not listed) and the hydrogen-bonding interactions are different, because in LT-IIb Lys213 of the A2 helix interacts with two carbonyl atoms of loop 24–34 (see Fig. 1b) while in LT-I it is Gln215 that interacts with the carbonyl atom of Tyr33 and Nη1 atom of Arg33 [6]. Although the proposed conformational changes in [6] are speculative, the fact that the nature of these two important interactions required for the activation pathway is conserved in the new LT-IIb structure strengthens this hypothesis.

Compared to LT-I and CT, LT-IIa and LT-IIb have a lower affinity for model substrates such as the guanidinium-containing agmatine [19]. However, $G_s\alpha$ is a good substrate for both the type I and type II enterotoxins. Concerning a possible binding site for $G_s\alpha$, it is noteworthy that there is a stretch of residues which has been shown by mutagenesis studies to be critical for enzymatic activity [37,40]. These residues, Tyr104, Pro106, and His107, are located on the other side of the active site crevice to the residues we discussed in the previous paragraphs. Thus, one could speculate that they are important for binding the second substrate, $G_s\alpha$. However, in the absence of an A1–substrate complex, we refrain from attempts to explain the substrate specificity similarities and differences based on the latent LT-IIb and LT-I structures.

B-subunit structure in the cholera toxin family

The striking similarity between the structures of the B subunits of LT-IIb and LT-I is evident from Figure 3b. A superposition of 81 equivalent Cα atoms results in an rms deviation of 1.6 Å. The internal disulfide bond between Cys10 and Cys81 is located at the same position in LT-IIb as in LT-I. The largest difference can be found in the N terminus; in LT-IIb the N-terminal helix is almost a full turn longer than that observed in LT-I. A structure- based sequence alignment (Fig. 6) reveals that the sequence identity is restricted to 11 out of 99 residues situated in

Figure 6

Structure based sequence alignment of the B subunits of members of the AB_5 toxin family. Sequences are aligned from LT-IIb, LT-IIa, human LT-I1, human LT-I2 (with the His13→Arg mutation), porcine LT-I, CT1 (E1 Tor strain), CT2 (classical strain) and verotoxin-1 (VT1). Sequences were taken from [69]. The residues which form the solvent accessible pore are shown in yellow and the residues that form the hydrophobic core within a single B subunit are in green. The subset of pore residues, that form the hydrophobic region of the pore, are shown in boxed regions and the residues that are at the conserved B–B interface in LT-IIb are indicated by a '^' symbol. The N-terminal helix is not included in the residue classification since this helix is not present in VT1. The secondary structure symbols are indicated above the sequence according to the LT-IIb structure. Residues found in structurally equivalent positions in the corresponding crystal structures are underlined (for the Shiga toxin [SHT] B subunit, coordinates of VT1 [70] were used instead of the SHT coordinates as the latter are not available in the PDB). The residues that are not structurally equivalent are also included in this figure to show the composition and length of these loop residues.

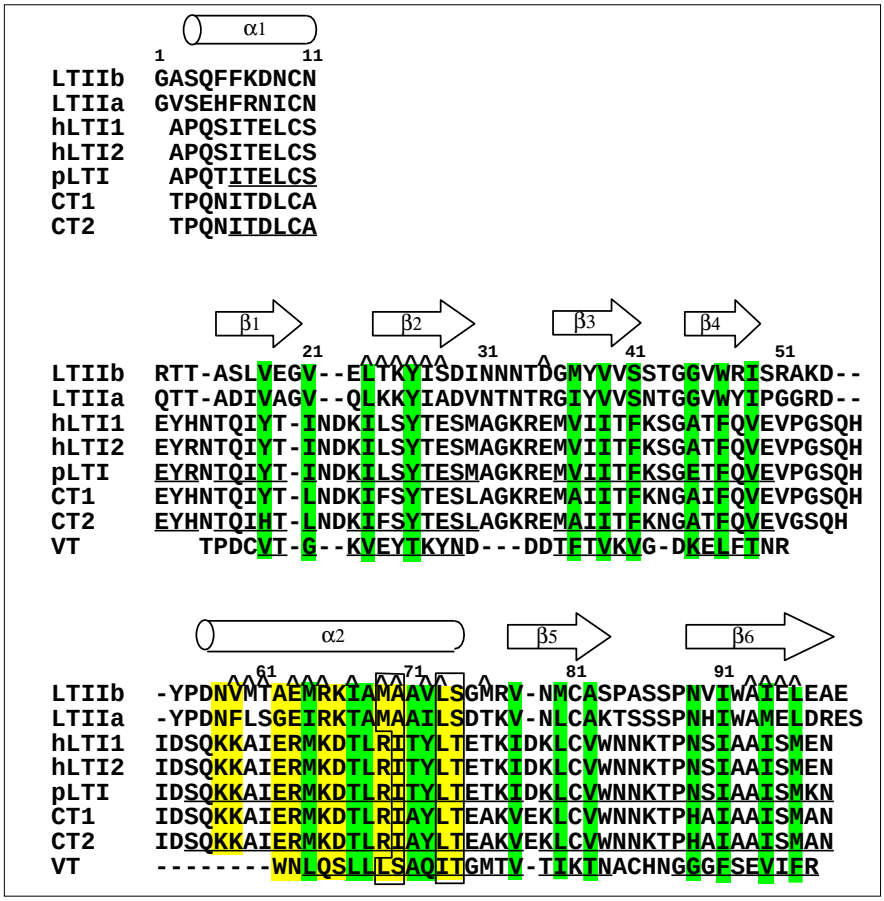

structurally equivalent positions. There are three gaps in the LT-IIb structure when compared to the LT-I B subunit, which is four residues longer. The structural similarity between the LT-IIb and LT-I B subunits also extends beyond the monomer B subunit. The superposition of the B pentamers of these toxins results in an rms deviation of 1.9 Å for 5×81 Cα atoms. The B subunits in the two toxins again provide an example of close structural similarities of proteins without much correspondence in sequence.

The individual B subunits within the LT-IIb pentamer are very similar to each other: the rms deviation between the structures ranges from 0.24 to 0.34 Å for Cα atoms. The largest differences are observed near residue 33, a region with high thermal mobility resulting in poor electron density in 4 out of 5 B subunits. Despite these differences, the individual B subunits of LT-IIb are very similar to each other in structure and have great similarity in thermal motion (not shown).

Receptor binding of LT-IIb

Concerning the binding site for the receptor of LT-IIb, G_{D1a}, several lines of evidence point to a region similar to the ganglioside-binding pocket in LT-I. First, the hydroxyl atoms of both Thr13 and Thr14 have been found critical for G_{D1a} affinity [45]; second, the postulated G_{D1a} binding site is in agreement with the location where most proteins with the oligonucleotide/oligosaccharide-binding fold (OB-fold) bind their nucleotide or saccharides [46]; third, Thr13 and Thr14 are located in a loop lining a pocket with Trp92 located at the base of the pocket (Fig. 7a), a feature that has been observed in LT-I as well as in other galactose-binding sites [5]. In LT-I it is Trp88 that provides an important hydrophobic interaction with the hydrophobic side of the galactose moiety of G_{M1}. The single tryptophan residue in LT-I and LT-IIb are sequentially not in equivalent positions, as the Cα of Ser83 in LT-IIb occupies the position equivalent to the Cα of Trp88 in LT-I (Fig. 7b). Nevertheless, structurally, the side chains of the tryptophan residues are in an identical location, although they have different orientations (Fig. 7b). The presence of the hydrophobic face of Trp92 in close proximity to Thr13 and Thr14 forming a pocket suggests that this concave protein region is involved in recognition of G_{D1a}.

On the basis of the unliganded structure of LT-IIb, it seems that Thr13 and Thr14 have different roles in maintaining the ability of LT-IIb to bind G_{D1a}. The hydroxyl

Figure 7

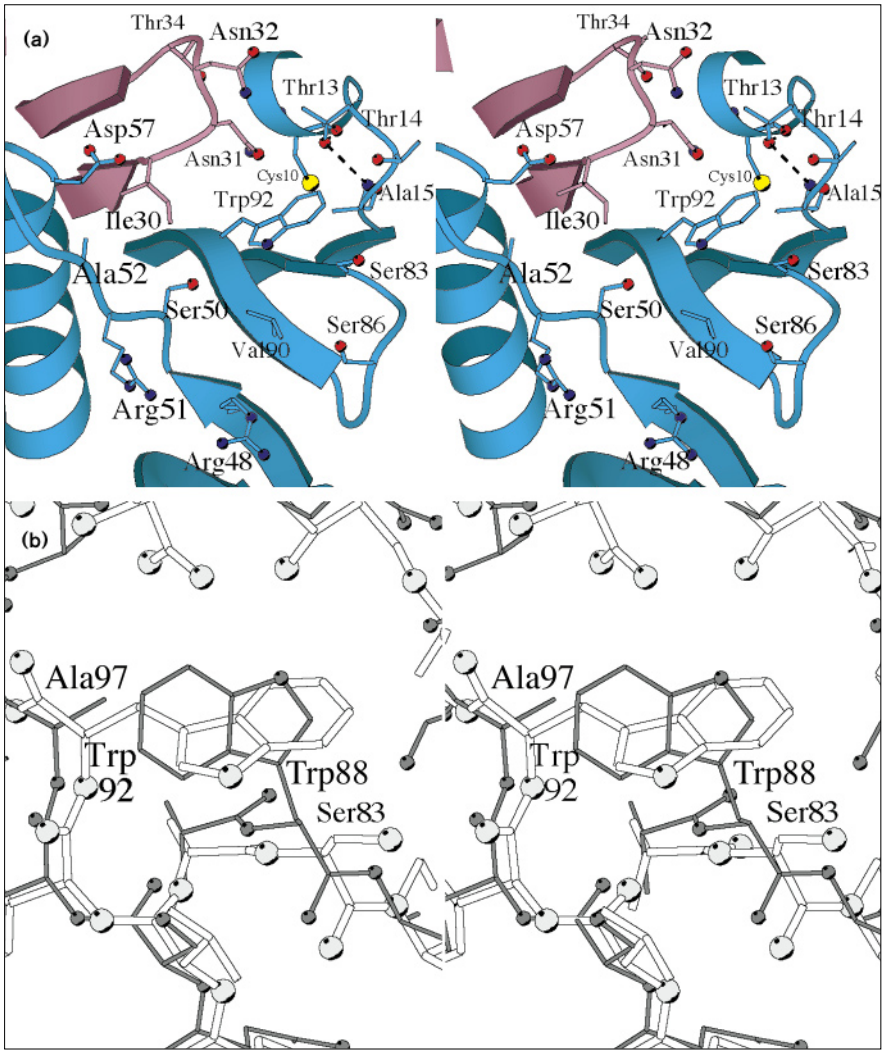

Receptor binding site. (a) Stereo diagram showing the putative G_{D1a} binding site located in the B subunit. The critical residues Thr13 and Thr14 are indicated. Trp92 and other neighboring residues are also shown. The figure shows two adjacent B subunits, one colored blue and the other purple. Sulphur, oxygen and nitrogen atoms are represented as yellow, red and blue spheres, respectively. (b) Stereo diagram showing a close-up of the galactose binding site of LT-I and the proposed ganglioside binding site of LT-IIb after superposition of the B subunits. LT-I is shown in dark ball-and-stick representation while LT-IIb is shown in white ball-and-stick. Trp88 and Trp92 of LT-I and LT-IIb, respectively, are highlighted. The residues at the equivalent position of these tryptophans in LT-IIb and LT-I are Ser83 and Ala97, respectively.

group of Thr14 is solvent accessible, indicating that its importance is most likely in a direct or solvent-mediated interaction with G_{D1a}. Thr13, however, is involved in the formation of two hydrogen bonds with O of Cys10 and N of Ala15, suggesting a role in maintaining the structural integrity of important residues at the G_{D1a} binding site. In addition, the importance of conformational changes of LT-IIb upon receptor binding should not be ignored. For example, upon binding G_{M1} or fragments thereof, loop 51–60 becomes tightly ordered in LT-I [5,7].

Receptor binding of LT-IIa

The close sequence similarity of LT-IIa and LT-IIb allows an analysis of LT-IIa substitutions which affect the receptor-binding site in LT-IIa. In LT-IIa, receptor recognition is less specific than for LT-IIb as LT-IIa recognizes a larger variety of gangliosides, including G_{D1b}, G_{D1a}, and G_{M1} [20]. At least two gangliosides, G_{M1} and G_{D1b}, were shown to compete with each other, suggesting that they have spatially overlapping binding sites in LT-IIa [47]. Thr13 and Thr34 were found to be important for G_{D1b}, G_{D1a}, and G_{M1} binding in LT-IIa [47]. Thr14 was also found to be critical for G_{D1a} and G_{D1b} recognition, but it was less involved in G_{M1} binding as a Thr14→Ile variant still maintained G_{M1}-binding activity. Thr34 in LT-IIa seems to have a structural role, because mutations at this site cause a low efficiency of assembly as well as a loss of ganglioside binding [47]. This structural role is confirmed in the LT-IIb structure, as Thr34 makes two hydrogen bonds with Oδ1 of Asp29 and with Nδ2 of Asn33. In contrast, Thr34 in LT-IIb is not critical for G_{D1a} binding [44]. Thus, the receptor-binding sites in LT-IIa and LT-IIb are at the same location on the B pentamer, with critical roles being played by Thr13 and Thr14.

The remarkable differences in ganglioside specificity between LT-IIa and LT-IIb were studied using chimeric proteins that combine sequences from LT-IIa and LT-IIb

Figure 8

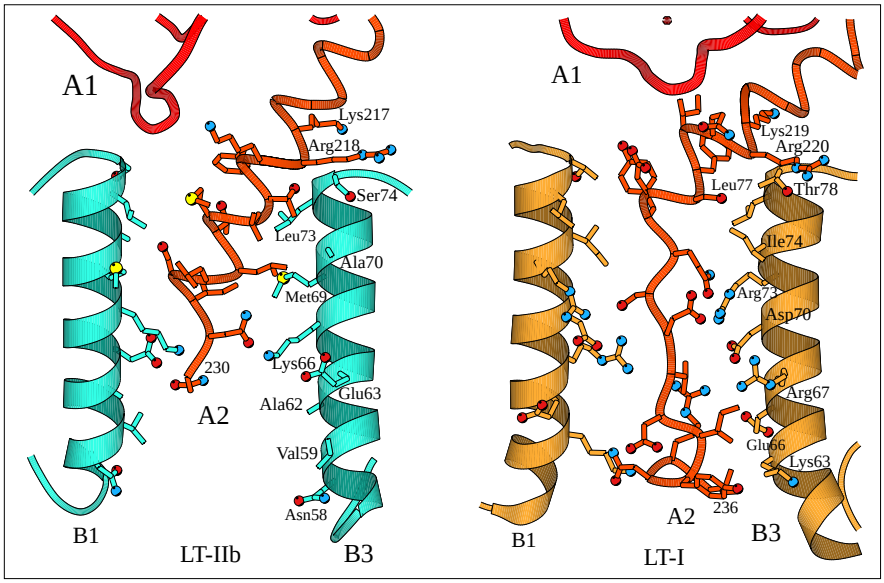

Close-up view of the A2 chains of LT-IIb and LT-I inside their corresponding B pentamer pore. LT-IIb is shown on the left, and LT-I [3,4] on the right. For clarity, only two of the five B subunits (B1 and B3) are shown, the B subunits are shown in blue and yellow for LT-IIb and LT-1 respectively. The model of LT-IIb A2 stops at residue 230 although some electron density could be observed lower in the channel for part of residues 231–243 of the A2 chain. In LT-I, the last four residues (237–240) of the A2 chain are also not shown as no electron density could be located for these residues. The A2 chain is shown in orange, while the A1 subunit is in red. Important residues involved in the A2–B pentamer interaction are indicated.

[45]. The N-terminal residues (1–53) of LT-IIa were found to determine the broader binding specificity for G_{D1b}, G_{D1a}, and G_{M1}, whereas residues 1–70 of LT-IIb determine the narrower binding specificity for G_{D1a} [45]. In light of these results, and to further address the issue of the differences in ganglioside specificity, 13 residues found in close proximity to the putative ganglioside G_{D1a} binding pocket of LT-IIb (Fig. 7a) were compared with the corresponding residues in LT-IIa [10,11]. It appears that 7 out of 13 of these residues are different in LT-IIa, with major differences at positions 48, 51 and 83 and more conservative changes at positions 30, 32, 50 and 52. All but one of these differences are situated within the aforementioned N-terminal region that determines the ganglioside specificity. Though the precise nature of the interactions of the two LT-IIs with their corresponding receptors still needs to be confirmed by other experiments, all the available evidence points to the ganglioside-binding site of LT-IIb to center around Trp92 (Fig. 7a).

Association of the A subunit with the B pentamer

Most interestingly, the mode of association of the A subunit with the B pentamer of LT-IIb is substantially different from that seen in the LT-I structure [3,4]. In LT-IIb the A2 helix continues as a helix into the pore, ending in the middle of the pore at residue 229 (Fig. 8). In LT-I, however, the A2 helix approaches the B pentamer from a different angle than that observed in LT-IIb. This different angle does not allow the A2 helix to extend into the pore of LT-I. Instead, the A2 polypeptide continues into the pore as an extended chain followed by a small helix at the other end of the pore [3,4] (Fig. 8). The residues forming the pore in LT-IIb are almost all different from those which form the pore in LT-I (Figs 6,8).

In LT-IIb, residue 230 is not part of the helix and residues 231–243 could not be fit in the uninterpretable electron density present in the lower half of the pore. The interactions between A2 and the B pentamer in the upper part of the pore are entirely hydrophobic in nature by means of Phe220, Thr221, Leu222, Met223, Thr224, Leu225, Leu226, and Ile228 of A2 interacting with Met69, Ala70, Leu73 and the Cβ of Ser74 of each of the B subunits. In fact, upon A2–B_5 association, a surface of 1127 Å^2 is buried, of which 869 Å^2 is hydrophobic. None of these A2–B interactions in LT-IIb are conserved in LT-I. The sequence of the part of the LT-IIb A2 chain which interacts with the B subunit bears hardly any sequence identity to that of LT-1 except for Lys217 and Arg218, which are located just above the pore in both enterotoxins (Fig. 8). The interactions of these two residues are different in LT-IIb and LT-I. In the middle of the pore there are several specific interactions observed between the A2 chain of LT-IIb and its B pentamer. Interestingly, all hydrogen-bond interactions are provided by the Nζ atom of Lys66 from three different B subunits which interact with five different oxygen atoms of the A2 subunit (Fig. 8).

The lower part of the pore holds the remaining 13 C-terminal residues, for which some electron density is present. Since the last interpretable residue (Asn230) is already two-thirds of the way down the 30 Å long pore (Fig. 8), it seems likely that not all 13 remaining residues will fit inside the lower part of the pore. The four C-terminal residues lysine, aspartate, glutamate, leucine (KDEL) in the A2 fragment of LT-IIb, being an endoplasmic reticulum (ER) retention signal [48], will thus most likely extend outside the pore, similar to the arginine, aspartate, glutamate, leucine (RDEL) terminus in LT-I [3,4]. The

equivalent KDEL sequence in CT is also located just outside the opening of the pore [8]. The involvement of the ER retention signal in LT intoxication has been postulated. However, recent studies have reached different conclusions concerning the role of RDEL/KDEL-dependent retrograde transport through the Golgi-ER during intoxication by CT and LT-I [49,50].

A common feature of pores in the AB_5 toxin family

The sequence comparison shown in Figure 6 highlights the residues forming the pore in all B_5-containing toxins. The bottom half of the pore, comprising residues 59, 62, 63 and 66 in LT-IIb, seems to be highly polar in all toxins with many charged residues pointing into the pore. The exception is Shiga toxin (SHT), which has polar but no charged residues. Clearly, the nature and distribution of the polar and charged residues in the lower half of the pore are not conserved and are completely different in various members of the toxin family. Surprisingly, in all toxin structures solved so far, not many specific interactions are made inside the pore between the linker of the A subunit and this hydrophilic lower half of the pore. In SHT [51] and LT-IIb, residues within this linker are too disordered in the bottom region within the pore to be modeled completely.

The upper region of the pore, however, comprises a conserved ring of hydrophobic residues present in all AB_5 toxin structures solved to date (Table 3). The solvent accessible hydrophobic surface in the upper region of the pore is large in all toxin pentamers (approximately 450–660 Å^2). Concerning the conserved hydrophobic region of the pore, the presence of the hydrophilic Ser42 in SHT and VT is the only exception within the AB_5 toxin family, giving rise to a somewhat smaller overall, but still dominant, hydrophobic accessible surface in VT compared to the other members of the family. The AB_5 complex formation of LT-IIb makes almost full use of this hydrophobic surface by complementing it with a hydrophobic region of the A2 helix, thus almost doubling the amount of buried hydrophobic surface mentioned above. Residue 74 of the B subunit of LT-IIb, which in all toxins is either serine or threonine (Fig. 6), is special as its Oγ atom is always involved in a hydrogen bond with the carbonyl oxygen of the residue one turn further down the central helix. This leaves the hydrophobic atom(s) of the serine and threonine residues at this position (residue Ser74 in LT-IIb and Thr78 in LT-I) pointing towards the interior of the pore (see Fig. 8).

The conserved ring of hydrophobic surface in the upper region of the pores within the diverse family of AB_5 toxins is intriguing. The interactions at the top part of the pore consist of a mainly hydrophobic area of the A2 helix interacting with the ring of hydrophobic residues at the top of the pore. Though it is not immediately obvious, there are several potential reasons why this feature might be conserved and they will be discussed individually.

Table 3

Solvent-accessible molecular surface: comparison of the upper region of the B-pentamer pore in related toxins.

Toxin	Solvent-accessible hydrophobic surface (Å^2)	Solvent-accessible hydrophilic surface (Å^2)	Residues involved
LT-IIb	494	0	Met69, Ala70, Leu73, Ser74
LT-I	658	5	Ile74, Leu77, Thr78
CT	549	25	Ile74, Leu77, Thr78
VT/SHT	449	117	Leu41, Ser42, Ile45, Thr46

The solvent accessible surface for the side chains forming the pore in the pentamer of LT-IIb and LT-I (PDB code 1LTS) were calculated after omitting the A subunit from the coordinate set. CT (PDB code 1CHB), and VT (PDB code 1BOV) B pentamers were used and all water molecules were omitted in the calculations. The program MSCON [67] was used for the solvent-accessible molecular calculations.

Overcoming the non-fivefold symmetry of the A2 chain

Since hydrophobic interactions are not usually very direction sensitive, the hydrophobic upper region within the pore allows the non-fivefold linker to interact with a pore possessing fivefold symmetry. In SHT [51], LT-IIb, and to a lesser extent LT-I, this interaction is achieved by means of a helix, with variable length, which is mainly hydrophobic. In LT-IIb and SHT [51] about 1130 and 1000 Å^2 of surface area are buried respectively, by insertion of the helix into the pore. The amount of solvent accessible surface area buried in LT-I in just the upper region of the pore (by A2 residues upto Ser228 [4]) is 1020 Å^2, of which 664 Å^2 is hydrophobic. Since the A2 helix in LT-I barely enters the pore, and A2 continues down the pore in an extended chain conformation, the amount of hydrophobic surface buried in the upper region of the pore is significantly smaller than in LT-IIb, although it is still substantial.

AB_5 assembly

The assembly of CT and LT-I holotoxin has been postulated to involve intermediates such as AB_3 and/or AB_4 [52]. The A subunit was found to only associate with B subunits that were in the process of assembling, and not with fully assembled B pentamers [53]. Such an assembly pathway has not yet been studied for LT-IIa, LT-IIb and SHT, their *in vitro* AB_5 assembly under non-denaturing conditions is possible but with a low efficiency [54,55]. The more efficient assembly *in vivo* of the latter toxins will thus most likely also involve association of the A subunit with B subunits that are not fully assembled B pentamers. The B_3 or B_4 subunit folding intermediate might thus attract the A subunit such that the partial hydrophobic ring at the upper part of the incomplete pore interacts with the hydrophobic part of the A2 linker. The middle and lower parts of the long central helices of the B subunits might be involved in more specific hydrophilic interactions with the A2 linker in these AB_3 or AB_4 assembly

intermediates. It has also been suggested that the interactions of the A subunit with the not fully assembled B subunits enhance the stability of the assembly intermediate in LT-I [53], thus resulting in the ability of its A subunit to accelerate the rate of B subunit pentamerization. The toxin AB_3 or AB_4 assembly intermediates can now attract single B subunits to favourably complement the remaining part of the exposed hydrophobic A2 helix with the top part of their central B subunit helix: additional B–B and B–A2 subunit interactions complete the assembly process.

In conclusion, we propose that the hydrophobic ring present in the upper region of the pore in all AB_5 toxins is conserved since it can facilitate interaction of a fivefold symmetry containing molecule with a non-fivefold symmetric, yet helical and hydrophobic, A2 linker. We also propose that the hydrophobic ring aids in the *in vivo* AB_5 assembly involving AB_3 and/or AB_4 intermediates.

Hybrid toxins

The above mentioned similarities and differences concerning the A2–B_5 interactions within the family of AB_5 toxins may explain the results observed in *in vivo* complementation studies with A and B subunits from type I and type II enterotoxins. A subunits of LT-IIa and LT-IIb are able to form hybrid toxins *in vivo* with B subunits of LT-I, although with low efficiency [54]. This is remarkable, as the sequence similarity in the A2 region between the type II and the type I heat-labile enterotoxins is very limited. The A2 chain of LT-IIa or LT-IIb is thus able to assemble not only with its own B pentamer but also with the B pentamer of LT-I that has only 11% sequence identity and significantly different pore characteristics. However, as the majority of the interactions between the A2 helix and the B pentamer in LT-IIb holotoxin involve non-specific but complementary hydrophobic interactions in the conserved upper region of the pore, it seems likely that such interactions also occur in the hybrid toxin formed by an A subunit of LT-II and a B subunit of LT-I.

The 'inverse' hybrid, consisting of the A subunit of LT-I and the B subunit of either LT-IIa or LT-IIb, did not assemble *in vivo* [54]. As described above, the A2 linker of LT-I does not complement the hydrophobic surface within the pore of B_5 as efficiently as the A2 linker of LT-IIb. The A2 fragment of LT-I in this region is much more hydrophilic than that of LT-IIb. Instead the A2–B_5 interactions in LT-I holotoxin are spread throughout the entire length of the pore, involving more interactions unique to LT-I. With this in mind, the inability of the LT-I A subunit to associate with B pentamers of LT-IIa and LT-IIb is not surprising.

Hybridization studies using AB_5 bacterial toxins have also been successfully carried out with toxins that are more homologous than LT-I and LT-II. The A and B subunits of Shiga-like toxin-I (SLT-I) and SLT-II *in vitro* can, under denaturing conditions, be assembled into hybrid toxins [56]. Likewise, A subunits of SHT and SLT-I can both form hybrid toxin *in vivo* with B subunits of SLT-II and SLT-IIv [57]. In addition, hybrid toxins between LT-I and CT have been obtained both *in vivo* and *in vitro* under denaturing conditions [53,58] as well as hybrids between LT-IIa and LT-IIb, again both *in vivo* and *in vitro* under non-denaturing conditions [54]. In all these hybrid holotoxins, the residues involved in the A–B_5 interface are not fully conserved compared to the corresponding wild type holotoxins. Taken together, the results obtained with assembly of hybrid toxins in several systems described above, suggest that the AB_5 assembly process is quite promiscuous. This is in agreement with the fact that the upper hydrophobic part of the pore is common to, and plays a crucial role in assembly in all these pore-containing AB_5 toxins.

Conserved hydrophobic core of B subunits among the AB_5 toxin family

The CT family (consisting of CT variants, LT-I variants, LT-IIa and LT-IIb) are members of a large family of so called 'AB_5 toxins' [59,60] including pertussis toxin (which is not included in the sequence alignment in Figure 6 since it contains a hetero B pentamer), SHT and SLT (also called verotoxin). Figure 6 highlights the positions (shown in green) that are part of the common hydrophobic core in the B subunits of the structures solved so far in the AB_5 toxin family. Although not a single residue is conserved in all of the sequences, the hydrophobic nature of these residues forming the core is highly conserved. The conservation of hydrophobicity is less noticeable in the B–B interface residues (Fig. 6) than in the residues forming the core of a single B subunit. The structure based sequence alignment of the quite divergent B subunits of members of the AB_5 toxins reveals the presence of a conserved hydrophobic core, and might be useful in the identification of future members of the AB_5 toxin family that contain B subunits with a similar fold.

Biological implications

The heat-labile enterotoxin family consists of ADP-ribosylating toxins with an AB_5 structure. These toxins elevate cAMP levels by activating adenylate cyclase in the small intestine of susceptible animals, thereby inducing the secretion of fluids and electrolytes resulting in diarrhea. Cholera toxin (CT) and the type I heat-labile enterotoxins (LT-I) of *E. coli* are antigenically related whereas the type II heat-labile enterotoxins of *E. coli* (LT-II) are antigenically distinct from the type I enterotoxins. Although CT and LT-I have been clearly demonstrated to be significant causes of diarrhea, the role of LT-II in diarrheal diseases of humans and other animals has not yet been established. The catalytic A subunit of LT-IIb, like CT and LT-I, activates

adenylate cyclase by ADP-ribosylation of a G protein subunit, $G_s\alpha$. The structure of LT-IIb at the atomic level can aid in understanding the still unknown ADP-ribosylation mechanism of the toxin family. In addition, the fact that the quaternary structure of LT-IIb closely resembles that of LT-I and CT advances our understanding of the folding of the individual polypeptides and in particular the assembly into AB_5 holotoxin.

The structure of the catalytic domain of LT-IIb is very similar to the catalytic domain structures of LT-I and CT. This is in agreement with their 60% sequence identity, but the close structural similarity also suggests that the low pH of 4.4 used for LT-IIb crystallization, does not alter the active site in the A subunit.

The B subunit of LT-IIb, which is responsible for recognition of the ganglioside G_{D1a} receptor, adopts a fold similar to that of LT-I and other members of this toxin family, despite the very limited sequence identity of 11%. In AB_5 type toxins B subunits come together to form a doughnut shaped pentamer with a central pore. The ganglioside receptor binding sites in LT-IIb are in a similar region of the pentamer to the receptor-binding sites in LT-I and CT. Comparison of all known toxin pentamer structures revealed the presence of a conserved hydrophobic ring of solvent accessible surface in the upper region of the pore. This finding offers a structural explanation for the observation that certain combinations of A and B subunits from type I and type II enterotoxins are able to form hybrid toxins. We propose that this hydrophobic upper half of the pore plays a crucial role in AB_5 assembly in the periplasm of the pathogens producing these toxins. Clearly, the B pentamers of the cholera toxin family are the result of divergent evolution during which the ring-like shape of the B pentamer, the general position for recognizing carbohydrate moieties of receptors, and the hydrophobic upper part of the pore have all been conserved as crucial common features.

Materials and methods

Protein purification and crystallization

Previous methods [16] were improved by using a recombinant bacterial strain and richer growth medium to overproduce LT-IIb and by modifying the purification procedures. Plasmid pTC100 contains a 1.68 Kbp *Bgl*II-*Hpa*I fragment, from pCP4185 encoding LT-IIb [11], ligated into pBluescript KS$^+$. The LT-IIb operon is oriented so that it can be expressed from the strong *lac* promoter of the vector. In a representative experiment, *E. coli* HB101 (pTC100) was grown at 37°C and 250 rotations per min (rpm) to an optical density at 600nm (OD_{600})=1.4. The culture was grown in 4 l Erlenmeyer flasks containing 1 l amounts of medium (35 g tryptone, 20 g yeast extract, 5 g NaCl, 75 mg ampicillin and 50 mg kanamycin per l at pH 7.5). Isopropyl-β-D-thiogalactopyranoside (IPTG) was added to each culture at 0.5 mM final concentration, and incubation was continued for an additional 19 h. All further procedures were performed at 4°C. The bacteria from 12 flasks (112 g wet weight) were collected by centrifugation and disrupted by sonication. The purification scheme involved ammonium sulfate precipitation at 60% saturation, ion exchange chromatography on DEAE-cellulose, chromatofocussing on PBE94, and gel filtration chromatography on Sephadex G100. The final yield of purified LT-IIb was 88 mg at 8.8 mg=ml^{-1}, and the purified LT-IIb appeared homogeneous as assessed by SDS-page. LT-IIb was then concentrated to about 10 mg=ml^{-1} using the Centricon system (10 kDa). LT-IIb was crystallized using the sitting drop method from 2.0 M NaCl, 0.2 M Li_2SO_4, 0.2 M sodium acetate buffer at pH 4.7 and 4°C. The final pH of the reservoir is pH 4.4. Data collection size crystals grew in about 2–3 months with a smallest dimension of about 0.15 mm.

X-ray diffraction data

The first native data set and the Pt-derivative data set were collected at room temperature from a single crystal on an RAXIS-II image plate detector and processed using RAXIS-software from Molecular Structure Corporation (The Woodlands, Texas). The second native dataset was collected at the CHESS synchrotron facility to higher resolution, integrated using DENZO and scaled using SCALEPACK [61,62] (Table 1). This data set was used for the final stages of refinement. The spacegroup of the LT-IIb crystals is $P3_121$ with cell dimensions a=b=105.7 Å and c=171.6 Å.

Structure determination

An LT-IIb crystal was soaked for 24 h in a mother liquor containing 10 mM K_2PtCl_4. The derivative dataset was scaled to the native data set using KBRANI (WGJH and SC Mande, unpublished program). The first major platinum site was calculated by hand and verified using RSPS [63] and VSFUN4 (WGJH, unpublished program). The other six sites were determined using the cross search mode in RSPS as well as by calculating a cross difference Fourier using phases obtained from MLPHARE [64] with the single Pt site. Finally, all seven positions were refined using MLPHARE first with data from 15–5 Å resolution (Table 1) and later extended to 4.0 Å. Five of the seven atoms had inter Pt distances and angles that followed fivefold symmetry with two independent sites per B subunit. One site had three out of five possible platinum atoms bound and the other site had only two out of five bound per pentamer. A 5 Å resolution electron-density map using phases calculated from the Pt derivative, with an overall figure of merit of 0.34 for acentric reflections (without anomalous data), revealed five long rods along a fivefold axis which coincided with the fivefold axis obtained from the Pt sites (Fig. 1a). Also the A2 helix was clearly visible in this map (Fig. 1a). The helices from the B pentamer of LT-I surprisingly matched the five rods of density including their angle with the fivefold axis. It was this angle of the five rods with the fivefold axis with respect to the position of the A subunit that helped in determining the correct spacegroup enantiomer, $P3_121$. Solvent flattening and histogram matching using DM (K Cowtan, unpublished program) was used to improve the quality of the 5 Å map. Next, a polyalanine model of the LT-I B pentamer was placed in density as well as a homology model of the A subunit based upon the LT-I structure. O [65] was used to build this homology model, consisting of the A1 subunit and the helix portion of A2. The Cα coordinates of the pentamer after rigid body refinement in X-PLOR [26] were used to generate improved NCS operators. DM was then used to phase extend from 4 to 2.9 Å resolution using solvent flattening and histogram matching. IMP (GJ Kleywegt and TA Jones, unpublished program) was used to refine the NCS using a mask of a single B subunit yielding correlation coefficients of about 0.22. The uninterpretable 2.9 Å map was averaged using MAMA (GJ Kleytwegt and TA Jones, unpublished program) for 1 cycle. This averaged map could readily be interpreted with the scaffold of the LT-I B pentamer as a guide, assigning about 80% of the residues in the LT-IIb B subunit. The partial model of the B pentamer as well as the coordinates of the A subunit after the initial rigid body refinement were subjected to standard molecular dynamics, positional and individual temperature factor refinement in X-PLOR. The new coordinates of the B pentamer were used to obtain improved NCS operators to calculate an improved averaged map. $F_o–F_c$ and $2F_o–F_c$ maps were also calculated to model the remaining parts of the structure using O.

Refinement

Initially the native data set 1 was used for refinement. 5% of the data were set aside for the R_{free} before refinement. Iterative cycles of model building and refinement were performed as well as extending the resolution from 2.9 to 2.5 Å. PROCHECK [66] was used to identify residues with geometric strain that needed to be rebuilt. 46 solvent molecules were modeled with data from 10–2.5 Å resolution resulting in an R factor of 19.5% and an R_{free} of 26.6 %. The 2.25 Å native data set 2 was then used to complete the refinement with all data included. 215 solvent molecules were modeled that had electron-density features above 3σ in a F_o–F_c map and appropriate hydrogen-bonding interactions with the protein. At this point the crystallographic R factor was 19.7%. A final anisotropic overall B-factor refinement in X-PLOR brought the R factor to 19.1%. The six anisotropic B factor parameters were refined to the following values: U11=0.0410, U22=0.0410, U33=–0.0488, U12=0.0117, U13=0.0000, U23=0.0000. The anisotropy in the data was already visible during data collection. The quality of the final model was checked with PROCHECK, and the rms deviations from ideality are listed in Table 2. The average rms deviation comparing the Cα coordinates from the separate B subunits is about 0.29 Å.

Accession numbers

The coordinates of LT-IIb have been deposited with the Brookhaven Protein Data Bank (entry code 1TII).

Note added in proof

After submission of this manuscript a paper describing the NAD-binding mode to DT and recognizing the conservation of Gly34, which is the equivalent of Gly19 in LT-IIb as described in this paper, in the family of ADP-ribosylating toxins has appeared in press [44].

Acknowledgements

We would like to thank Shekhar Mande for his help concerning the programs RSPS, DM and VSFUN4. These investigations were supported by NIH Grant AI-14107 from the National Institute of Allergy and Infectious Disease (to RKH) and NIH Grant AI34501 from the same institute (to WGJH). WGJH acknowledges a major equipment grant from the Murdock Charitable Trust. We would also like to thank CHESS and their supporting staff for their help.

References

1. Spangler, B.D. (1992). Structure and function of cholera toxin and the related *Escherichia coli* heat-labile enterotoxin. *Microbiol. Rev.* **56**, 622–647.
2. Hol, W.G.J., Sixma, T.K. & Merritt, E.A. (1995). Structure and function of *E. coli* heat-labile enterotoxin and cholera toxin B pentamer. In *Handbook of Natural Toxins.* (Moss, J., Iglewski, B., Vaughan, M. and Tu, A.T., eds), vol. 8, pp. 185–215, Marcel Dekker, Inc., New York, NY.
3. Sixma, T.K., *et al.*, & Hol, W.G.J. (1991). Crystal structure of a cholera toxin-related heat-labile enterotoxin from *E. coli. Nature* **351**, 371–377.
4. Sixma, T.K., *et al.*, & Hol, W.G.J. (1993). Refined structure of *Escherichia coli* heat-labile enterotoxin, a close relative of cholera toxin. *J. Mol. Biol.* **230**, 890–918.
5. Merritt, E.A., Sixma, T.K., Kalk, K.H., van Zanten, B.A.M. & Hol, W.G.J. (1994). Galactose-binding site in *Escherichia coli* heat-labile enterotoxin (LT) and cholera toxin (CT). *Mol. Microbiol.* **13**, 745–753.
6. van den Akker, F., Merritt, E.A., Pizza, M., Domenighini, M., Rappuoli, R. & Hol, W.G.J. (1995). The Arg7Lys mutant of heat-labile enterotoxin exhibits great flexibility of active site loop 47–56 of the A subunit. *Biochemistry* **34**, 10996–11004.
7. Merritt, E.A., Sarfaty, S., van den Akker, F., L'Hoir, C., Martial, J.A. & Hol, W.G.J. (1994). Crystal structure of cholera toxin B-pentamer bound to receptor G_{M1} pentasaccharide. *Protein Sci.* **3**, 166–175.
8. Zhang, R.-G., *et al.*, & Westbrook, E.M. (1995). The three-dimensional crystal structure of cholera toxin. *J. Mol. Biol.* **251**, 563–573.
9. Green, B.A., Neill, R.J., Ruyechan, W.T. & Holmes, R.K. (1983). Evidence that a new enterotoxin of *Escherichia coli* which activates adenylate cyclase in eucaryotic target cells is not plasmid mediated. *Infect. Immun.* **41**, 383–390.
10. Pickett, C.L., Weinstein, D.L. & Holmes, R.K. (1987). Genetics of type IIa heat-labile enterotoxin of *Escherichia coli*: operon fusions, nucleotide sequence, and hybridization studies. *J. Bacteriol.* **169**, 5180–5187.
11. Pickett, C.L., Twiddy, E.M., Coker, C. & Holmes, R.K. (1989). Cloning, nucleotide sequence, and hybridization studies of the type IIb heat-labile enterotoxin gene of *Escherichia coli*. *J. Bacteriol.* **171**, 4945–4952.
12. Seriwatana, J., *et al.*, & Clayton, C.L. (1988). Type II heat-labile enterotoxin-producing *Escherichia coli* isolated from animals and humans. *Infect. Immun.* **56**, 1158–1161.
13. Celemin, C., Anguita, J., Naharro, G. & Suarez, S. (1994). Evidence that *Escherichia coli* isolated from the intestine of healthy pigs hybridize with LT-II, ST-Ib and SLT-II DNA probes. *Microb. Pathog.* **16**, 77–81.
14. Guth, B.E.C., *et al.*, & Trabulsi, L.R. (1986). Production of type II heat-labile enterotoxin by *Escherichia coli* isolated from food and human faeces. *Infect. Immun.* **59**, 587–589.
15. Holmes, R.K., Twiddy, E.M. & Pickett, C.L. (1986). Purification and characterization of type II heat-labile enterotoxin of *Escherichia coli. Infect. Immun.* **53**, 464–473.
16. Guth, B.E.C., Twiddy, E.M., Trabulsi, L.R. & Holmes, R.K. (1986). Variation in chemical properties and antigenic determinants among type II heat-labile enterotoxins of *Escherichia coli. Infect. Immun.* **54**, 529–536.
17. Donta, S.T., Tomicic, T. & Holmes, R.K. (1992). Binding of class II *Escherichia coli* enterotoxins to mouse Y1 and intestinal cells. *Infect. Immun.* **60**, 2870–2873.
18. Chang, P.P., Moss, J., Twiddy, E.M. & Holmes, R.K. (1987). Type II heat-labile enterotoxin of *Escherichia coli* activates adenylate cyclase in human fibroblasts by ADP ribosylation. *Infect. Immun.* **55**, 1854–1858.
19. Lee, C.-M., *et al.*, & Holmes, R.K. (1991). Activation of *Escherichia coli* heat-labile enterotoxins by native and recombinant adenosine diphosphate-ribosylation factors, 20-kD guanine nucleotide-binding proteins. *J. Clin. Invest.* **87**, 1780–1786.
20. Fukuta, S., Magnani, J.L., Twiddy, E.M., Holmes, R.K. & Ginsburg, V. (1988). Comparison of the carbohydrate-binding specificities of cholera toxin and *Escherichia coli* heat-labile enterotoxins LTh-I, LT-IIa, and LT-IIb. *Infect. Immun.* **56**, 1748–1753.
21. Ladish, S., Becker, H. & Ulsh, L. (1992). Immunosuppression by human gangliosides: I. Relationship of carbohydrate structure to the inhibition of T cell responses. *Biochim. Biophys. Acta.* **1125**, 180–188.
22. Morton, D.L., Ravindranath, M.H. & Irie, R.F. (1994). Tumor gangliosides as targets for active specific immunotherapy of melanoma in man. *Progr. Brain Res.* **101**, 251–275.
23. Reisfeld, R.A., Mueller, B.M., Handgretinger, R., Yu, A.L. & Gillies, S.D. (1994). Potential of genetically engineered anti-ganglioside G_{D2} antibodies for cancer immunotherapy. *Progr. Brain Res.* **101**, 201–212.
24. Marxen, P., Erdmann, G. & Bigalke, H. (1991). The translocation of botulinum A neurotoxin by chromaffin cells is promoted in low ionic strength solution and is insensitive to trypsin. *Toxicon* **29**, 181–189.
25. Epand, R.M., Nir, S., Parolin, M. & Flanagan, T.D. (1995). The role of the ganglioside G_{D1a} as a receptor for Sendai virus. *Biochemistry* **34**, 1084–1089.
26. Brünger, A.T., Kuriyan, J. & Karplus, M. (1987). Crystallographic R factor refinement by molecular dynamics. *Science* **235**, 458–460.
27. Okamoto, K., Takatori, R., Okamoto, K. (1995). Effect of substitution for arginine residues near position 146 of the A subunit of *Escherichia coli* heat-labile enterotoxin on the holotoxin assembly. *Microbiol. Immunol.* **39**, 193–200.
28. Sixma, T.K., Aguirre, A., Terwisscha van Scheltinga, A.C., Warnta, E.S., Kalk, K.H. & Hol, W.G.J. (1992). Heat-labile enterotoxin crystal forms with variable A/B_5 orientation. *FEBS Lett.* **305**, 81–85.
29. Lencer, W.I., Strohmeier, G., Moe, S., Carlson, S.L., Constable, C.T. & Madara, J.L. (1995). Signal transduction by cholera toxin: processing in vesicular compartments does not require acidification. *Am. J. Physiol.* **269** (*Gastrointest. Liver Physiol.* **32**), G548–G557.
30. Janicot, M., Fouque, F. & Desbuquois, B. (1991). Activation of rat liver adenylate cyclase by cholera toxin requires toxin internalization and processing in endosomes. *J. Biol. Chem.* **266**, 12858–12865.
31. Tsuji, T., Inoue, T., Miyama, A., Okamoto, K., Honda, T. & Miwatani, T. (1990). A single amino acid substitution in the A subunit of *Escherichia coli* enterotoxin results in a loss of its toxic activity. *J. Biol. Chem.* **265**, 22520–22525.
32. Tsuji, T., Inoue, T., Miyama, A. & Noda, M. (1991). Glutamic acid-112 of the A subunit of heat-labile enterotoxin from enterotoxigenic *Escherichia coli* is important for ADP-ribosyltransferase activity. *FEBS Lett.* **291**, 319–321.

33. Hase, C.C., *et al.*, & Finkelstein, R.A. (1994). Construction and characterization of recombinant *Vibrio cholerae* strains producing inactive cholera toxin analogs. *Infect. Immun.* 62, 3051–3057.
34. Lobet, Y., Cluff, C.W. & Cieplak, W., Jr. (1991). Effect of site-directed mutagenic alterations on ADP-ribosyltransferase activity of the A subunit of *Escherichia coli* heat-labile enterotoxin. *Infect. Immun.* 59, 2870–2879.
35. Burnette, W.N., *et al.*, & Kaslow, H.R. (1991). Site-specific mutagenesis of the catalytic subunit of cholera toxin: substituting lysine for arginine 7 causes loss of activity. *Infect. Immun.* 59, 4266–4270.
36. Harford, S., Dykes, C.W., Hobden, A.N., Read, M.J. & Halliday, I.J. (1989). Inactivation of the *Escherichia coli* heat-labile enterotoxin by *in vitro* mutagenesis of the A-subunit gene. *Eur. J. Biochem.* 183, 311–316.
37. Pizza, M., *et al.*, & Rappuoli, R. (1994). Probing the structure-activity relationship of *Escherichia coli* LT-A by site-directed mutagenesis. *Mol. Microbiol.* 14, 51–60.
38. Kaslow, H.R., Platler, B., Takada, T., Moss, J., Mar, V.L. & Burnette, W.N. (1992). Effects of site-directed mutagenesis of cholera toxin A1 subunit ADP-ribosyltransferase activity. In *Bacterial Protein Toxins*, *Zentralblatt fur Bakteriologie Suppl.* 23, 197–198.
39. Vadheim, K.L., Singh, Y. & Keith, J.M. (1994). Expression and mutagenesis of recombinant cholera toxin A subunit. *Microb. Pathog.* 17, 339–346.
40. Fontana, M.R., *et al.*, & Pizza, M. (1995). Construction of nontoxic derivatives of cholera toxin and characterization of the immunological response against the A subunit. *Infect. Immun.* 63, 2356–2360.
41. Li, M., Dyda, F., Benhar, I., Pastan, I. & Davies, D.R. (1995). The crystal structure of *Pseudomonas aeruginosa* exotoxin domain III with nicotinamide and AMP: conformational differences with the intact exotoxin. *Proc. Natl. Acad. Sci. USA* 92, 9308–9312.
42. Bennett, M.J. & Eisenberg, D. (1994). Refined structure of monomeric diphtheria toxin at 2.3 Å resolution. *Protein Sci.* 3, 1464–1475.
43. Stein, P.E., Boodhoo, A., Armstrong, G.D., Cockle, S.A., Klein, M.H. & Read, R.J. (1994). The crystal structure of pertussis toxin. *Structure* 2, 45–57.
44. Bell, C.E. & Eisenberg, D. (1996). Crystal structure of diphtheria toxin bound to nicotinamide adenine dinucleotide. *Biochemistry* 35, 1137–1149.
45. Connell, T.D. & Holmes, R.K. (1995). Mutational analysis of the ganglioside-binding activity of the type II *Escherichia coli* heat-labile enterotoxin LT-IIb. *Mol. Microbiol.* 16, 21–31.
46. Murzin, A.G. (1993). OB(oligonucleotide/oligosaccharide binding)-fold: common structural and functional solution for non-homologous sequences. *EMBO J.* 12, 861–867.
47. Connell, T.D. & Holmes, R.K. (1992). Molecular genetic analysis of ganglioside GD1b-binding activity of *Escherichia coli* type IIa heat-labile enterotoxin by use of random and site-directed mutagenesis. *Infect. Immun.* 60, 63–70.
48. Pelham, H.R. (1989). Control of protein exit from the endoplasmic reticulum. *Annu. Rev. Cell Biol.* 5, 1–23.
49. Cieplak, W., Jr., Messer, R.J., Konkel, M.E. & Grant, C.C.R. (1995). Role of a potential endoplasmic reticulum retention sequence (RDEL) and the Golgi complex in the cytotonic activity of *Escherichia coli* heat-labile enterotoxin. *Mol. Microbiol.* 16, 789–800.
50. Lencer, W.I., *et al.*, & Holmes, R.K. (1995). Targeting of cholera toxin and *Escherichia coli* heat-labile toxin in polarized epithelia: role of COOH-terminal KDEL. *J. Cell Biol.* 131, 951–962.
51. Fraser, M.E., Chernaia, M.M., Kozlov, Y.V. & James, M.N.G. (1994). Crystal structure of the holotoxin from *Shigella dysenteriae* at 2.5 Å resolution. *Nat. Struct. Biol.* 1, 59–64.
52. Hirst, T.R. (1994). Biogenesis of cholera toxin and related oligomeric enterotoxins. In *Handbook of Natural Toxins.* (Moss, J., Iglewski, B., Vaughan, M. and Tu, A.T., eds), vol. 8, pp. 123–184, M. Dekker, Inc., NY.
53. Hardy, S.J.S., Holmgren, J., Johansson, S., Sanchez, J. & Hirst, T.R. (1988). Coordinated assembly of multisubunit proteins: oligomerization of bacterial enterotoxins *in vivo* and *in vitro*. *Proc. Natl. Acad. Sci. USA* 85, 7109–7113.
54. Connell, T.D. & Holmes, R.K. (1992) Characterization of hybrid toxins produced in *Escherichia coli* by assembly of A and B polypeptides from type I and type II heat-labile enterotoxins. *Infect. Immun.* 60, 1653–1661.
55. Austin, P.R., Jablonski, P.E., Bohach, G.A., Dunker, A.K. & Hovde, C.J. (1994). Evidence that the A2 fragment of shiga-like toxin type I is required for holotoxin integrity. *Infect. Immun.* 62, 1768–1775.
56. Ito, H., Yutsudo, T., Hirayama, T. & Takeda, Y. (1988). Isolation and some properties of A and B subunits of vero toxin 2 and *in vitro* formation of hybrid toxins between subunits of vero toxin 1 and vero toxin 2 from *Escherichia coli* O157: H7. *Microb. Pathog.* 5, 189–195.
57. Weinstein, D.L., Jackson, M.P., Perera, L.P., Holmes, R.K. & O'Brien, A.D. (1989). *In vivo* formation of hybrid toxins comprising shiga toxin and the shiga-like toxins and role of the B subunit in localization and cytotoxic activity. *Infect. Immun.* 57, 3743–3750.
58. Takeda, Y., Honda, T., Taga, S. & Miwatani, T. (1981). *In vitro* formation of hybrid toxins between subunits of *Escherichia coli* heat-labile enterotoxin and those of cholera enterotoxin. *Infect. Immun.* 34, 341–346.
59. Merritt, E.A. & Hol, W.G.J. (1995). AB_5 toxins. *Curr. Opin. Struct. Biol.* 5, 165–171.
60. Burnette, W.N. (1994). AB_5 ADP-ribosylating toxins: comparative anatomy and physiology. *Structure* 2, 151–158.
61. Otwinowski, Z. (1990). DENZO. A program for automatic evaluation of film densities. Yale University, New Haven, CT.
62. Minor, W. (1993). XDISPLAYF Program, Purdue University, USA.
63. Knight, S. (1989). Ribulose 1,5-bisphosphate carboxylase/oxygenase – a structural study [PhD Thesis]. Swedish University of Agricultural Sciences, Uppsala, Sweden.
64. Otwinowski, Z. (1991). Maximum likelihood refinement of heavy atom parameters. In *Isomorphous Replacement and Anomalous Scattering.* (Wolf, W., Evans, P.R. & Leslie, A.G.W., eds), pp. 80–86, SERC Daresbury Laboratory, Warrington, UK.
65. Jones, T.A., Zou, J.-Y., Cowan, S.W. & Kjeldgaard, M. (1991). Improved methods for building protein models in electron density maps and the location of errors in these models. *Acta Cryst. A* 47, 110–119.
66. Laskowski, R.A., MacArthur, M.W., Moss, D.S. & Thornton, J.M. (1993). PROCHECK: a program to check the stereochemical quality of protein structures. *J. Appl. Cryst.* 26, 283–291.
67. Connolly, M.L. (1983). Analytical molecular surface calculations. *J. Appl. Cryst.* 16, 548–558.
68. Kraulis, P.J. (1991). MOLSCRIPT: a program to produce both detailed and schematic plots of protein structures. *J. Appl. Cryst.* 24, 946–950.
69. Domenighini, M., Pizza, M., Jobling, M.G., Holmes, R.K. & Rappuoli, R. (1995). Identification of errors among database sequence entries and comparison of correct amino acid sequences for the heat-labile enterotoxins of *Escherichia coli* and *Vibrio cholerae*. *Mol. Microbiol.* 15, 1165–1167.
70. Stein, P.E., Boodhoo, A., Tyrrell, G.J., Brunton, J.L. & Read, R.J. (1992). Crystal structure of the cell-binding B oligomer of verotoxin-1 from *E. coli*. *Nature* 355, 748–750.